EUROFUSION WP14ER-PR(16) 16697

N Horsten et al.

Assessment of fluid neutral models for an ITER detached case including atomic databases and reflection model

Preprint of Paper to be submitted for publication in
Nuclear Fusion

This work has been carried out within the framework of the EUROfusion Consortium and has received funding from the Euratom research and training programme 2014-2018 under grant agreement No 633053. The views and opinions expressed herein do not necessarily reflect those of the European Commission.

Assessment of fluid neutral models for an ITER detached case including atomic databases and reflection model

N. Horsten[1], G. Samaey[2] and M. Baelmans[1]

[1] KU Leuven, Department of Mechanical Engineering, Celestijnenlaan 300A, 3001 Leuven, Belgium

[2] KU Leuven, Department of Computer Science, Celestijnenlaan 200A, 3001 Leuven, Belgium

E-mail: `niels.horsten@kuleuven.be`

March 2016

Abstract.

We assess different fluid neutral models by comparing the resulting plasma sources to the sources from a Monte Carlo simulation of the kinetic equation. The background plasma is kept fixed and represents an ITER detached case. The fluid models take into account the microscopic cross-sections and rate coefficients from the AMJUEL-HYDHEL databases and the microscopic TRIM reflection model. We accomplish the latter by elaborating macroscopic fluxes that are imposed as boundary conditions, without the introduction of any user-defined fitting parameters. The pure pressure-diffusion equation provides accurate results for the particle source, but is inaccurate for the parallel momentum and ion energy source. Therefore, we have added a parallel momentum equation. This gives maximum errors of about 9% for the momentum and 32% for the energy source. These errors are further reduced to respectively 6 and 14% by adding a separate neutral energy equation. It is hard to ascertain whether the remaining fluid-kinetic discrepancies are either mainly due to numerical or modeling errors.

Keywords: plasma edge modeling, neutrals, fluid approximation

1. Introduction

Plasma edge codes are crucial for the design of the divertor, pumps and other plasma-facing components. The neutral particles are mostly described kinetically, where the kinetic equation is solved with a Monte Carlo (MC) simulation with codes such as EIRENE [1]. However, the statistical noise hampers the convergence and the calculation time increases for charge-exchange (CX) dominated regimes due to the high number of ion-neutral collisions. With the traditional MC approach it is excluded to use

gradient-based optimization techniques to obtain an optimal design for, e.g., the divertor geometry [2].

Therefore, there is a need for (partially) deterministic neutral models, e.g., a fluid model that becomes valid in high-collisional regions. Multiple fluid neutral models that strongly differ in terms of performance, have been developed over the last decades. The most simple fluid neutral model in literature consists of a diffusion model based on density gradients, assuming mono-energetic neutrals [3] or using a multi-group approach [4]. This model is improved by solving a pressure-diffusion equation [5–8]. The pressure-diffusion equation is obtained by neglecting the convective and viscous terms in the Navier-Stokes (momentum) equations, which results immediately in an expression for the particle flux. Imposing this expression in the continuity equation leads to a single convection-diffusion equation. A parallel momentum equation is added in Refs. [6,9–11] and the full Navier-Stokes model with the momentum equations in the three directions is solved in Refs. [6, 12].

The largest difficulties occur due to the choice of the boundary conditions, which are very influential for the results and have to represent the underlying physics. This becomes especially an issue for the more complete models due to the additional boundary conditions for the extra equations. A typical boundary condition for the parallel momentum equation is the momentum recycling boundary condition where the neutral parallel velocity at the target plate is assumed to be a constant fraction of the ion parallel velocity [6, 10]. However, this fraction is user-defined and not based on the underlying physics. In addition, flux limiters are often used to model the non-equilibrium behavior and mimic the results from the kinetic solution [5, 8, 10, 11, 13]. This leads to models with multiple user-defined case-specific fitting parameters that are not determined by a theoretical or empirical law.

In this paper, we develop a hierarchy of fluid neutral models with different degrees of complexity starting from the Boltzmann (kinetic) equation. We also derive the boundary conditions starting from the kinetic description. This leads to imposed boundary fluxes for the fluid models. Therefore, we need the velocity distribution of the incident neutrals at the boundaries. This distribution is estimated with the help of the diffusion theory from Ref. [14]. In addition, we incorporate the AMJUEL-HYDHEL atomic databases [15, 16] for collision processes and the TRIM code database [17], which contains all information about the energy and angular distributions of reflected particles as a function of the incident energy and angle for different projectile-solid material combinations. This leads to fluid neutral models that are as much as possible consistent with the underlying microscopic description without the use of artificial fitting parameters as, e.g., the momentum recycling and flux limiter coefficients.

A sufficiently accurate fluid neutral model can replace the MC simulation for studies where the details of all microscopic physics of the neutrals are not that important, e.g., for the development of operational scenarios for a certain machine and to investigate other physical phenomena. It is important that the sources from the neutral-plasma interactions are of the same order of magnitude as the sources from an MC simulation

and that the same trends can be observed. In this way the computational cost can be limited and there is no noise that hampers the convergence. An accurate fluid neutral model can lead to a significant speed-up of design calculations with plasma edge codes. If still more accurate results are desired, a well-performing fluid neutral model is the basis for an efficient hybrid approach, where a kinetic correction is added to the fluid model, as, e.g., proposed in Ref. [18].

This paper is outlined as follows. In Section 2, we elaborate the fluid neutral models starting from the kinetic equation. The treatment from the boundary conditions is discussed in Section 3. Finally, in Section 4 we assess the fluid neutral models by comparing the results to an MC simulation of the kinetic equation with a fixed background plasma. Exclusively the outer divertor leg from ITER is modeled and the plasma is taken from a (partially) detached case.

2. From a kinetic to fluid description

2.1. Kinetic model

We only consider Deuterium (D) atoms. The (steady-state) kinetic neutral equation becomes

$$\begin{aligned}\mathbf{v}\cdot\nabla f_{\mathrm{n}}(\mathbf{v}) = \widetilde{f}_{\mathrm{i}}(\mathbf{v})n_{\mathrm{i}}n_{\mathrm{e}}K_{\mathrm{r}} + n_{\mathrm{i}}\int\sigma_{\mathrm{cx}}(E_{\mathrm{c}})||\mathbf{v}-\mathbf{v}'||\widetilde{f}_{\mathrm{i}}(\mathbf{v})f_{\mathrm{n}}(\mathbf{v}')\mathrm{d}\mathbf{v}' \\ - f_{\mathrm{n}}(\mathbf{v})(n_{\mathrm{i}}K_{\mathrm{cx}}(\mathbf{v}) + n_{\mathrm{e}}K_{\mathrm{i}}),\end{aligned} \tag{1}$$

with $\mathbf{v}$ the neutral particle velocity vector, $\nabla = \nabla_{\mathbf{x}}$ the gradient with respect to the position $\mathbf{x}$, $f_{\mathrm{n}}(\mathbf{v})$ the neutral velocity distribution function and $\widetilde{f}_{\mathrm{i}}(\mathbf{v})$ the normalized ion distribution ($\int\widetilde{f}_{\mathrm{i}}(\mathbf{v})\mathrm{d}\mathbf{v} = 1$), which is assumed to be a drifting Maxwellian. The short notation $\int\ldots\mathrm{d}\mathbf{v}$ is used for the integral over the whole velocity space (thus for all velocity components from $-\infty$ to ∞). The ion, electron and neutral densities are respectively n_{i}, n_{e} and $n_{\mathrm{n}} = \int f_{\mathrm{n}}(\mathbf{v})\mathrm{d}\mathbf{v}$.

The left hand side of the equation describes the neutral transport while the sources and sinks, due to the interactions with ions and electrons, are stated in the right hand side. Three processes are taken into account: volumetric (radiative and three-body) recombination, electron impact ionization and CX collisions with respectively rate coefficients K_{r}, K_{i} and K_{cx}. Due to the large thermal velocity of the electrons compared to the ion and neutral thermal velocity, the recombination and ionization rate coefficients are independent of the particle velocity. This is no longer the case for the CX rate coefficient, due to the similar thermal velocity of both collision partners (ions and neutrals). Consequently, the rate coefficient becomes a function of the particle velocity $\mathbf{v}$, given by

$$K_{\mathrm{cx}}(\mathbf{v}) = \int\sigma_{\mathrm{cx}}(E_{\mathrm{c}})||\mathbf{v}-\mathbf{v}'||\widetilde{f}_{\mathrm{i}}(\mathbf{v}')\mathrm{d}\mathbf{v}', \tag{2}$$

with $\sigma_{\mathrm{cx}}(E_{\mathrm{c}})$ the microscopic cross-section, which is a function of the center-of-mass kinetic energy of the collision partners $E_{\mathrm{c}} = \frac{m}{4}||\mathbf{v}-\mathbf{v}'||^2$, with m the particle mass. The expressions for K_{r}, K_{i} and σ_{cx} are taken from the AMJUEL-HYDHEL databases [15,16].

It should be noted that all distributions, densities and rate coefficients are functions of the spatial position.

2.2. Fluid models

As shown in Ref. [19], solving the following simplified Boltzmann equation leads to almost the same results as the exact Boltzmann equation (Eq. (1)), at least for a detached ITER case:

$$\mathbf{v}\cdot\nabla f_{\mathrm{n}}(\mathbf{v}) \approx \widetilde{f}_{\mathrm{i}}(\mathbf{v})n_{\mathrm{i}}n_{\mathrm{e}}K_{\mathrm{r}} - f_{\mathrm{n}}(\mathbf{v})n_{\mathrm{e}}K_{\mathrm{i}} + (\widetilde{f}_{\mathrm{i}}(\mathbf{v})n_{\mathrm{n}} - f_{\mathrm{n}}(\mathbf{v}))n_{\mathrm{i}}K_{\mathrm{cx,m}}, \tag{3}$$

making use of the so-called momentum linearized CX rate coefficient $K_{\mathrm{cx,m}}$. From now on, Eq. (3) is used for the derivation of the fluid neutral models.

The fluid equations are obtained by taking moments of the kinetic equation (Eq. (3)). If we generalize the kinetic equation as $\mathbf{v}\cdot\nabla f_{\mathrm{n}}(\mathbf{v}) = S(f_{\mathrm{n}}(\mathbf{v}))$, the continuity, momentum and (total) energy equations follow from the moments:

$$\int \mathbf{m}(\mathbf{v})\left(\mathbf{v}\cdot\nabla f_{\mathrm{n}}(\mathbf{v})\right)\mathrm{d}\mathbf{v} = \int \mathbf{m}(\mathbf{v})S(f_{\mathrm{n}}(\mathbf{v}))\mathrm{d}\mathbf{v}, \tag{4}$$

with $\mathbf{m}(\mathbf{v}) = \begin{bmatrix}1 & m\mathbf{v}^T & \frac{m}{2}||\mathbf{v}||^2\end{bmatrix}^T$. Elaborating this, gives

$$\nabla\cdot\mathbf{\Gamma}^{\mathrm{n}} = \nabla\cdot(n_{\mathrm{n}}\mathbf{V}_{\mathrm{n}}) = S_{n_{\mathrm{n}}}, \tag{5}$$

$$\nabla\cdot\Gamma^{\mathrm{n}}_{\mathrm{m,f}} = \nabla\cdot(mn_{\mathrm{n}}\mathbf{V}_{\mathrm{n}}\mathbf{V}_{\mathrm{n}} + \Pi_{\mathrm{n}}) = -\nabla p_{\mathrm{n}} + \mathbf{S}_{m\mathbf{V}_{\mathrm{n}}}, \tag{6}$$

$$\nabla\cdot\mathbf{Q}^{\mathrm{n}} = \nabla\cdot\left(\left(\frac{5}{2}T_{\mathrm{n}} + m\frac{||\mathbf{V}_{\mathrm{n}}||^2}{2}\right)n_{\mathrm{n}}\mathbf{V}_{\mathrm{n}} + \Pi_{\mathrm{n}}\cdot\mathbf{V}_{\mathrm{n}} + \mathbf{q}_{\mathrm{n}}\right) = S_{E,\mathrm{n}}, \tag{7}$$

solved for the neutral density n_{n}, drift velocity $\mathbf{V}_{\mathrm{n}} = \frac{1}{n_{\mathrm{n}}}\int \mathbf{v}f_{\mathrm{n}}(\mathbf{v})\mathrm{d}\mathbf{v} = \begin{bmatrix}u_{\mathrm{n}\theta} & u_{\mathrm{n}r} & u_{\mathrm{n}\phi}\end{bmatrix}^T$ and neutral temperature $T_{\mathrm{n}} = \frac{1}{n_{\mathrm{n}}}\frac{m}{3}\int ||\mathbf{c}||^2 f_{\mathrm{n}}(\mathbf{v})\mathrm{d}\mathbf{v}$, with $\mathbf{c} = \mathbf{v} - \mathbf{V}_{\mathrm{n}}$ the deviation from the drift velocity. The velocity $\mathbf{V}_{\mathrm{n}}$ is expressed in the poloidal (θ), radial (r), toroidal (ϕ) coordinate system. The stress tensor $\Pi_{\mathrm{n}} = m\int \mathbf{cc}f_{\mathrm{n}}(\mathbf{v})\mathrm{d}\mathbf{v} - p_{\mathrm{n}}\mathbb{I}$, with $p_{\mathrm{n}} = n_{\mathrm{n}}T_{\mathrm{n}}$ the neutral pressure and $\mathbb{I}$ the identity tensor, and the heat flux vector $\mathbf{q}_{\mathrm{n}} = \frac{m}{2}\int ||\mathbf{c}||^2\mathbf{c}\mathrm{d}\mathbf{v}$ have still to be determined.

Thus far, Eqs. (5)-(7) are fully equivalent with the kinetic equation. However, due to the presence of the unknown stress tensor and heat flux vector, the system cannot be solved. We need an expression for Π_{n} and $\mathbf{q}_{\mathrm{n}}$. Therefore, we use the Chapman-Enskog theory [20] that is valid for sufficiently small deviations of $f_{\mathrm{n}}(\mathbf{v})$ from the equilibrium distribution. The neutrals obtain the equilibrium distribution if the CX mean free path is much smaller than the macroscopic length scales determined by the gradients of relevant plasma properties (density, temperature, ...). In our case the fluid models are exclusively based on the neutral-ion CX collisions. No neutral self-collisions are taken into account for both kinetic and fluid models. Because of the assumed Maxwellian distribution for the ions, the neutral equilibrium distribution becomes also a Maxwellian.

The Chapman-Enskog approximation gives

$$\Pi_{\mathrm{n}} = -\eta^{\mathrm{n}}\left(\nabla\mathbf{V}_{\mathrm{n}} + (\nabla\mathbf{V}_{\mathrm{n}})^T - \frac{2}{3}(\nabla\cdot\mathbf{V}_{\mathrm{n}})\,\mathbb{I}\right), \tag{8}$$

$$\mathbf{q}_{\mathrm{n}} = -\kappa^{\mathrm{n}}\nabla T_{\mathrm{n}}, \tag{9}$$

with the viscosity $\eta^{\mathrm{n}} = \frac{n_{\mathrm{n}}T_{\mathrm{n}}}{n_{\mathrm{i}}K_{\mathrm{cx,m}}}$ and heat conduction coefficient $\kappa^{\mathrm{n}} = \frac{5n_{\mathrm{n}}T_{\mathrm{n}}}{2mn_{\mathrm{i}}K_{\mathrm{cx,m}}}$. As a rule of thumb, one can state that the Chapman-Enskog approximation is valid for Knudsen numbers (ratio of the CX mean free path and a characteristic macroscopic length scale) smaller than 0.1.

Also the particle flux density vector $\mathbf{\Gamma}^{\mathrm{n}}$, (fluid) momentum flux density tensor $\Gamma^{\mathrm{n}}_{\mathrm{m,f}}$ and energy flux density vector $\mathbf{Q}^{\mathrm{n}}$ are explicitly written down in Eqs. (5)-(7). The subscript f is used to distinguish between the momentum flux tensor from the fluid approach, which does not include the pressure, and the momentum flux tensor from the kinetic approach, defined as $\Gamma^{\mathrm{n}}_{\mathrm{m}} = m\int \mathbf{v}\mathbf{v}f_{\mathrm{n}}(\mathbf{v})\mathrm{d}\mathbf{v} = mn_{\mathrm{n}}\mathbf{V}_{\mathrm{n}}\mathbf{V}_{\mathrm{n}} + \Pi_{\mathrm{n}} + p_{\mathrm{n}}\mathbb{I}$. The latter includes the pressure. This distinction is important for the elaboration of the boundary condition of the momentum equation (Section 3.3.2).

The source terms are

$$S_{n_{\mathrm{n}}} = n_{\mathrm{i}}n_{\mathrm{e}}K_{\mathrm{r}} - n_{\mathrm{n}}n_{\mathrm{e}}K_{\mathrm{i}}, \tag{10}$$

$$\mathbf{S}_{m\mathbf{V}_{\mathrm{n}}} \approx m(n_{\mathrm{i}}n_{\mathrm{e}}K_{\mathrm{r}} + n_{\mathrm{n}}n_{\mathrm{i}}K_{\mathrm{cx,m}})\mathbf{V}_{\mathrm{i}} - m(n_{\mathrm{n}}n_{\mathrm{e}}K_{\mathrm{i}} + n_{\mathrm{n}}n_{\mathrm{i}}K_{\mathrm{cx,m}})\mathbf{V}_{\mathrm{n}}, \tag{11}$$

$$\begin{aligned} S_{E,\mathrm{n}} \approx{}& (n_{\mathrm{i}}n_{\mathrm{e}}K_{\mathrm{r}} + n_{\mathrm{n}}n_{\mathrm{i}}K_{\mathrm{cx,m}})\left(\frac{3}{2}T_{\mathrm{i}} + \frac{m}{2}||\mathbf{V}_{\mathrm{i}}||^2\right) \\ &- (n_{\mathrm{n}}n_{\mathrm{e}}K_{\mathrm{i}} + n_{\mathrm{n}}n_{\mathrm{i}}K_{\mathrm{cx,m}})\left(\frac{3}{2}T_{\mathrm{n}} + \frac{m}{2}||\mathbf{V}_{\mathrm{n}}||^2\right), \end{aligned} \tag{12}$$

with T_{i} the ion temperature and $\mathbf{V}_{\mathrm{i}} = \begin{bmatrix} u_\theta & u_r & u_\phi \end{bmatrix}^T = \begin{bmatrix} b_\theta u_{||} & 0 & \sqrt{1-b_\theta^2}u_{||} \end{bmatrix}^T$ the ion fluid velocity, with b_θ the magnetic pitch and $u_{||}$ the plasma parallel velocity. We assume that the plasma flows perfectly in the parallel direction. From Eq. (11) it can be seen that the momentum source due to CX collisions is linear with the ion-neutral fluid velocity difference if the moment from the simplified Boltzmann equation (Eq. (3)) is taken. In fact it is not perfectly linear, if the moment from the exact Boltzmann equation (Eq. (1)) should be taken, but the assumption is justified if the neutral distribution is close to a drifting Maxwellian. Thus, the momentum linearized CX rate coefficient $K_{\mathrm{cx,m}}$ is defined as the slope of the CX momentum source with respect to the ion-neutral velocity difference, as explained in more detail in Ref. [19]. Also the expression for the energy source (Eq. (12)) is the second order moment from the right hand side of the approximate Boltzmann equation (Eq. (3)) instead of from the exact kinetic equation (Eq. (1)).

The Navier-Stokes neutral model without the energy equation with the assumption of thermal equilibrium of neutrals and ions (Eqs. (5)-(6) with $T_{\mathrm{n}} = T_{\mathrm{i}}$) is frequently used in the late nineties (e.g., Ref. [21]). Due to the low Knudsen numbers in detached cases, it is a representative model to study the trends and behavior of the plasma in these regimes. However, solving the full system of Navier-Stokes equations with the

momentum equations in the three directions can become computationally costly and it is often hard to converge to the steady-state solution [22]. For practical calculations, it is recommended to reduce the model. We investigate three models with increasing degrees of complexity. They are elaborated in next subsections.

2.2.1. Model 1: pressure-diffusion equation In CX dominated regions, it is expected that the neutral dynamics is governed by a balance between the momentum source and the pressure gradient. Therefore, the left hand side of Eq. (6) (convective and viscous terms) becomes negligible, leading to a simplified momentum equation:

$$m(n_\mathrm{i}n_\mathrm{e}K_\mathrm{r} + n_\mathrm{n}n_\mathrm{i}K_\mathrm{cx,m})\mathbf{V}_\mathrm{i} - m(n_\mathrm{e}K_\mathrm{i} + n_\mathrm{i}K_\mathrm{cx,m})n_\mathrm{n}\mathbf{V}_\mathrm{n} = \nabla p_\mathrm{n}. \tag{13}$$

If we rearrange the terms, we get an expression for the particle flux density $\mathbf{\Gamma}^\mathrm{n}$:

$$\mathbf{\Gamma}^\mathrm{n} = n_\mathrm{n}\mathbf{V}_\mathrm{n} = n_\mathrm{n,eq}\mathbf{V}_\mathrm{i} - D_p^\mathrm{n}\nabla p_\mathrm{n}, \tag{14}$$

with $n_\mathrm{n,eq} = (n_\mathrm{i}n_\mathrm{e}K_\mathrm{r} + n_\mathrm{n}n_\mathrm{i}K_\mathrm{cx,m})/(n_\mathrm{i}K_\mathrm{cx,m} + n_\mathrm{e}K_\mathrm{i})$ and $D_p^\mathrm{n} = (m\,(n_\mathrm{i}K_\mathrm{cx,m} + n_\mathrm{e}K_\mathrm{i}))^{-1}$. Imposing this expression in the continuity equation leads to the so-called pressure-diffusion equation:

$$\nabla \cdot \left(n_\mathrm{n,eq}\mathbf{V}_\mathrm{i} - D_p^\mathrm{n}\nabla p_\mathrm{n}\right) = S_{n_\mathrm{n}}. \tag{15}$$

This single convection-diffusion equation combines the continuity (Eq. (5)) and momentum (Eq. (13)) equations and is solved for the neutral pressure. In addition, we assume that the neutrals are in thermal equilibrium with the ions ($T_\mathrm{n} = T_\mathrm{i}$). The pressure-diffusion equation is frequently used [5–8]. The model is linear with respect to the neutral pressure and consequently, it is easily solved.

2.2.2. Model 2: pressure-diffusion and parallel momentum equation The toroidal neutral velocity resulting from the pressure-diffusion equation $u_\mathrm{n\phi,PD}$ is

$$u_\mathrm{n\phi,PD} = \frac{n_\mathrm{n,eq}}{n_\mathrm{n}}u_\phi. \tag{16}$$

The toroidal contribution of the pressure gradient disappears due to the assumption of toroidal symmetry. $n_\mathrm{n,eq}$ tends to n_n for $K_\mathrm{cx,m} \gg K_\mathrm{i}, K_\mathrm{r}$ leading to almost equal neutral and ion toroidal velocities in CX dominated regions. Indeed, if the CX mean free path is small compared to the macroscopic length scales, the neutral fluid velocity will tend to the ion velocity. However, at the boundaries neutral particles are emitted in different directions as described by the underlying recycling/reflection model. This leads to an ion-neutral velocity difference close to the boundaries. It is from crucial importance to capture this velocity difference in order to get accurate results for the parallel momentum source for the plasma. Therefore, we add a momentum equation

parallel to the magnetic field:

$$\frac{1}{h_\phi\sqrt{g}}\frac{\partial}{\partial\theta}\left(\frac{h_\phi\sqrt{g}}{h_\theta}\left(mn_{\mathrm{n}}u_{\mathrm{n}\theta}u_{\mathrm{n}||}-\eta^{\mathrm{n}}\left(\frac{1}{h_\theta}\frac{\partial u_{\mathrm{n}||}}{\partial\theta}-u_{\mathrm{n}||}\frac{1}{h_\theta h_\phi}\frac{\partial h_\phi}{\partial\theta}\right)\right)\right) + \frac{1}{h_\phi\sqrt{g}}\frac{\partial}{\partial r}\left(\frac{h_\phi\sqrt{g}}{h_r}\left(mn_{\mathrm{n}}u_{\mathrm{n}r}u_{\mathrm{n}||}-\eta^{\mathrm{n}}\left(\frac{1}{h_r}\frac{\partial u_{\mathrm{n}||}}{\partial r}-u_{\mathrm{n}||}\frac{1}{h_r h_\phi}\frac{\partial h_\phi}{\partial r}\right)\right)\right) - mb_\theta n_{\mathrm{n}}u_{\mathrm{n}||}^2\frac{1}{h_\theta h_\phi}\frac{\partial h_\phi}{\partial\theta} = -b_\theta\frac{1}{h_\theta}\frac{\partial p_{\mathrm{n}}}{\partial\theta}+S_{mu_{\mathrm{n}||}}, \quad (17)$$

solved for the parallel neutral velocity $u_{\mathrm{n}||}=b_\theta u_{\mathrm{n}\theta}+\sqrt{1-b_\theta^2}u_{\mathrm{n}\phi}$. The metric coefficients are h_θ, h_r and h_ϕ and $\sqrt{g}=h_\theta h_r h_\phi$. $S_{mu_{\mathrm{n}||}}$ is the projection of the momentum source (Eq. (11)) in the parallel direction. This parallel momentum equation is similar to the parallel momentum equation for the plasma as described in Ref. [23] and implemented in, e.g., the SOLPS-ITER code package [24].

Eq. (17) is a simplified version of the exact parallel momentum equation as described in Ref. [25]. It is assumed that the neutral parallel velocity is at least an order of magnitude larger than the radial and diamagnetic components and only the dominant curvature terms are kept in the equation. The assumption of dominant parallel ion and neutral velocities can be violated in the presence of ion drifts. In addition, the viscous coupling in the three directions can lead to significant radial and diamagnetic neutral velocities, especially if neutral-neutral collisions are included. This has to be kept in mind for future extensions to the model.

Mainly the toroidal velocity is not well predicted by the pure pressure-diffusion equation close to the target (Eq. (16)) such that including a toroidal momentum equation should already lead to a sufficient improvement of the results. However, we choose for a parallel momentum equation, because this model can guarantee conservation of global parallel momentum of the plasma and the neutrals if the coupled plasma-neutral equations are solved. The parallel momentum equation for the neutrals is also solved in Refs. [6, 9, 10].

The parallel momentum equation is solved together with the continuity equation (Eq. (5)). The radial and diamagnetic particle flux densities follow from the pressure-diffusion equation:

$$n_{\mathrm{n}}u_{\mathrm{n}r} = -D_p^{\mathrm{n}}\frac{1}{h_r}\frac{\partial p_{\mathrm{n}}}{\partial r}, \quad (18)$$

$$n_{\mathrm{n}}u_{\mathrm{n}\perp} = -D_p^{\mathrm{n}}\sqrt{1-b_\theta^2}\frac{1}{h_\theta}\frac{\partial p_{\mathrm{n}}}{\partial\theta}, \quad (19)$$

with $u_{\mathrm{n}\perp}=\sqrt{1-b_\theta^2}u_{\mathrm{n}\theta}-b_\theta u_{\mathrm{n}\phi}$ the diamagnetic neutral velocity. For this model we still assume thermal equilibrium of the ions and the neutrals ($T_{\mathrm{n}}=T_{\mathrm{i}}$).

2.2.3. Model 3: pressure-diffusion, parallel momentum and energy equation For the last model we add a separate neutral energy equation to model 2 (Eqs. (5) and (17)). Elaborating Eq. (7), where we again assume the dominant neutral velocity in the parallel

direction, gives

$$\frac{1}{\sqrt{g}}\frac{\partial}{\partial\theta}\left(\frac{\sqrt{g}}{h_\theta}\left(\left(\frac{5}{2}T_\mathrm{n}+\frac{m}{2}u_{\mathrm{n}||}^2\right)n_\mathrm{n}u_{\mathrm{n}\theta}-\frac{\eta^\mathrm{n}}{2}\frac{1}{h_\theta}\frac{\partial}{\partial\theta}\left(u_{\mathrm{n}||}^2\right)+\eta^\mathrm{n}\frac{u_{\mathrm{n}||}^2}{h_\theta h_\phi}\frac{\partial h_\phi}{\partial\theta}-\kappa^\mathrm{n}\frac{1}{h_\theta}\frac{\partial T_\mathrm{n}}{\partial\theta}\right)\right)$$
$$+\frac{1}{\sqrt{g}}\frac{\partial}{\partial r}\left(\frac{\sqrt{g}}{h_r}\left(\left(\frac{5}{2}T_\mathrm{n}+\frac{m}{2}u_{\mathrm{n}||}^2\right)n_\mathrm{n}u_{\mathrm{n}r}-\frac{\eta^\mathrm{n}}{2}\frac{1}{h_r}\frac{\partial}{\partial r}\left(u_{\mathrm{n}||}^2\right)+\eta^\mathrm{n}\frac{u_{\mathrm{n}||}^2}{h_r h_\phi}\frac{\partial h_\phi}{\partial r}-\kappa^\mathrm{n}\frac{1}{h_r}\frac{\partial T_\mathrm{n}}{\partial r}\right)\right)$$
$$=S_{E,\mathrm{n}}. \quad (20)$$

Again, we make use of the pressure-diffusion expressions for the radial and diamagnetic particle flux densities (Eqs. (18)-(19)).

The assumption of different ion and neutral temperatures is innovative compared to the models from literature. For 1D cases it is already shown that the neutral energy equation improves the results [26].

3. Boundary conditions

Boundary conditions determine the solution of a partial differential equation. Therefore, it is important to elaborate them carefully such that they include as much as possible the microscopic physics. Particles incident on the solid material (e.g., the target plates) are reflected with a certain probability and the velocity distribution of the reflected particles is a function of the energy and angle with respect to the surface normal of the incoming particles.

There are two kinds of particles incident on the solid boundaries: ions that pick up electrons and recombine and neutral atoms. Both particles are re-emitted as neutrals (fast atoms or thermally released molecules). The recombined ions are called the recycled neutrals, while the other emitted particles are called the reflected neutrals. For the development of fluid boundary conditions that are consistent with the microscopic recycling/reflection model, we need the distribution of the incident neutrals and ions. The distribution of the incident neutrals is unknown and has to be estimated. We extend the diffusion theory elaborated in Ref. [14] to the two-dimensional plasma edge to estimate the incident neutral distribution, as explained in Section 3.1. The distribution of the incident ions is assumed to be a known truncated Maxwellian possibly accelerated by the sheath potential if the boundary is not parallel to the magnetic field. This distribution is elaborated in Section 3.2.

For known incident distributions the TRIM code database [17] can be applied to determine the distribution of the reflected particles. The TRIM database contains exclusively information about the fast recycled/reflected atoms. The probability of fast reflection as a function of incident energy and angle can be found in the TRIM tables. The remainder (or in some cases a fraction of the remainder) is thermally released as molecules (D_2), which are assumed to dissociate immediately by the Franck-Condon process. The dissociated atoms are emitted isotropically with an energy of 2 eV. The moments of the total velocity distribution (incident and recycled/reflected

particles) lead to fluxes, which are imposed as boundary fluxes for the fluid equations. The incorporation of the advanced TRIM reflection model for the calculation of these boundary fluxes is discussed in detail in Section 3.3.

3.1. Diffusion approximation to estimate the distribution of the incident neutrals

The diffusion theory is frequently used in nuclear (fission) reactor physics [27–29]. In our case, we will exclusively use it for estimating the distribution of the incident neutrals. We consider a control volume $\mathrm{d}V$ in which CX collisions scatter the neutrals in different directions, as indicated in Fig. 1. We are interested in the number of neutrals that reach the area $\mathrm{d}A$ spanned by the solid angle $\mathrm{d}\Omega$. $\mathrm{d}A$ is a surface element of the boundary (e.g., the target plate) with ν the coordinate axis in the direction of the inward pointing surface normal. Due to the toroidal symmetry the toroidal direction ϕ is always tangential to the boundary and τ is the other tangential direction perpendicular to ϕ.

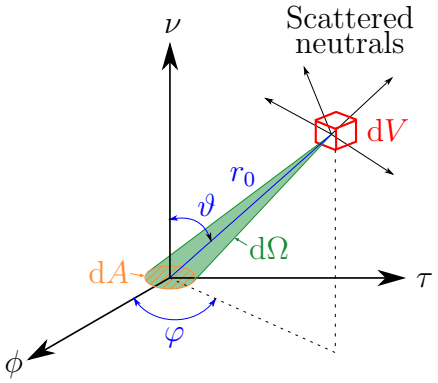

Figure 1. Scattering of neutrals in control volume $\mathrm{d}V$.

We try to calculate the velocity- and angular-dependent particle flux density $\Gamma^{\mathrm{n}}_{\nu-}(v,\vartheta,\varphi)$ of neutrals scattered by the ions and reaching the plane $\mathrm{d}A$. $\Gamma^{\mathrm{n}}_{\nu-}(v,\vartheta,\varphi)\mathrm{d}v\mathrm{d}\vartheta\mathrm{d}\varphi$ is the number of neutrals per m^2 per second reaching the surface element $\mathrm{d}A$ with a polar angle between ϑ and $\vartheta+\mathrm{d}\vartheta$, an azimuthal angle between φ and $\varphi+\mathrm{d}\varphi$ and a speed between v and $v+\mathrm{d}v$. This can be written as

$$\Gamma^{\mathrm{n}}_{\nu-}(v,\vartheta,\varphi)\mathrm{d}v\mathrm{d}\vartheta\mathrm{d}\varphi\mathrm{d}A=\int_{r_0=0}^{\infty}e^{-\Sigma_{\mathrm{t}}(v)r_0}n_{\mathrm{n}}n_{\mathrm{i}}K_{\mathrm{cx,m}}\widetilde{f}_{\mathrm{i}}(v,\vartheta,\varphi;0)\mathrm{d}V\mathrm{d}v\mathrm{d}\Omega. \tag{21}$$

$n_{\mathrm{n}}n_{\mathrm{i}}K_{\mathrm{cx,m}}\mathrm{d}V$ is the number of CX collisions per second in the volume element $\mathrm{d}V$ (at least if the simplified Boltzmann equation (Eq. (3)) is assumed to be true). These CX collisions are assumed to be the main origin for neutral particles at a certain distance r_0. The probability that the neutral gets a speed between v and $v+\mathrm{d}v$ and is scattered in $\mathrm{d}\Omega$ is $\widetilde{f}_{\mathrm{i}}(v,\vartheta,\varphi;0)\mathrm{d}v\mathrm{d}\Omega$, with $\widetilde{f}_{\mathrm{i}}(v,\vartheta,\varphi;\delta^{\mathrm{pot}}_{\mathrm{sh}})$ the normalized ion distribution (drifting

Maxwellian):

$$\widetilde{f}_{\mathrm{i}}(v,\vartheta,\varphi;\delta_{\mathrm{sh}}^{\mathrm{pot}}) = \left(\frac{m}{2\pi T_{\mathrm{i}}}\right)^{3/2} v^2 \exp\Bigg(- \frac{m}{2T_{\mathrm{i}}}\Bigg(v^2 + 2v\sin\vartheta\cos\varphi u_\phi + 2v\sin\vartheta\sin\varphi u_\tau + 2\sqrt{v^2\cos^2\vartheta - \frac{2}{m}\delta_{\mathrm{sh}}^{\mathrm{pot}}T_{\mathrm{e}}}u_\nu + u_\phi^2 + u_\tau^2 + u_\nu^2 - \frac{2}{m}\delta_{\mathrm{sh}}^{\mathrm{pot}}T_{\mathrm{e}}\Bigg)\Bigg), \tag{22}$$

with $\begin{bmatrix} u_\phi & u_\tau & u_\nu \end{bmatrix}^T$ the ion fluid velocity expressed in the (ϕ,τ,ν) coordinate system. The possible acceleration by the sheath potential, if the boundary is not parallel to the magnetic field, is already included in Eq. (22). The additional kinetic energy that the ion gets due to this acceleration is given by $\delta_{\mathrm{sh}}^{\mathrm{pot}}T_{\mathrm{e}}$, with T_{e} the electron temperature. Because of the assumption of an infinitesimal small sheath, this sheath acceleration plays only a role for the distribution of the incident ions (Section 3.2), whereas it is assumed that $\delta_{\mathrm{sh}}^{\mathrm{pot}} = 0$ for the sampling of the neutrals created by CX collisions ($\widetilde{f}_{\mathrm{i}}(v,\vartheta,\varphi;0)$ in Eq. (21)).

The source of CX neutrals has to be multiplied with the probability that the neutral reaches the boundary plane without any extra collision. This probability is represented by $e^{-\Sigma_{\mathrm{t}}(v)r_0}$, with $\Sigma_{\mathrm{t}}(v) = \frac{n_{\mathrm{i}}K_{\mathrm{cx,m}}+n_{\mathrm{e}}K_{\mathrm{i}}}{v}$ the total macroscopic cross-section (including CX and ionization events). We assume that the plasma background takes the whole domain up to $r_0 = \infty$. The solid angle spanned by $\mathrm{d}A$ is $\mathrm{d}A\frac{\cos\vartheta}{r_0^2}$ and the volume $\mathrm{d}V$ is $r_0^2\sin\vartheta\mathrm{d}r_0\mathrm{d}\vartheta\mathrm{d}\varphi$. Inserting these expressions in Eq. (21), gives

$$\Gamma_{\nu-}^{\mathrm{n}}(v,\vartheta,\varphi) = \int_{r_0=0}^{\infty} e^{-\Sigma_{\mathrm{t}}(v)r_0} n_{\mathrm{n}} n_{\mathrm{i}} K_{\mathrm{cx,m}} \widetilde{f}_{\mathrm{i}}(v,\vartheta,\varphi;0)\sin\vartheta\cos\vartheta\mathrm{d}r_0. \tag{23}$$

We use a Taylor series expansion for the neutral density:

$$n_{\mathrm{n}} \approx n_{\mathrm{n}_0} + \phi\left(\frac{\partial n_{\mathrm{n}}}{\partial\phi}\right)_0 + \tau\left(\frac{\partial n_{\mathrm{n}}}{\partial\tau}\right)_0 + \nu\left(\frac{\partial n_{\mathrm{n}}}{\partial\nu}\right)_0 \tag{24}$$

$$= n_{\mathrm{n}_0} + r_0\sin\vartheta\sin\varphi\left(\frac{\partial n_{\mathrm{n}}}{\partial\tau}\right)_0 + r_0\cos\vartheta\left(\frac{\partial n_{\mathrm{n}}}{\partial\nu}\right)_0, \tag{25}$$

assuming toroidal symmetry such that $\partial n_{\mathrm{n}}/\partial\phi = 0$. The subscript 0 indicates that the neutral density and gradients are evaluated in the origin where the particle flux density is calculated. Inserting this expression for the neutral density in Eq. (23) and evaluating the integral neglecting the spatial dependence of Σ_{t}, $n_{\mathrm{i}}K_{\mathrm{cx,m}}$ and $\widetilde{f}_{\mathrm{i}}$, gives

$$\Gamma_{\nu-}^{\mathrm{n}}(v,\vartheta,\varphi) = \frac{n_{\mathrm{i}}K_{\mathrm{cx,m}}}{n_{\mathrm{i}}K_{\mathrm{cx,m}} + n_{\mathrm{e}}K_{\mathrm{i}}}\widetilde{f}_{\mathrm{i}}(v,\vartheta,\varphi;0)v\sin\vartheta\cos\vartheta\Bigg(n_{\mathrm{n}} + \frac{v}{n_{\mathrm{i}}K_{\mathrm{cx,m}} + n_{\mathrm{e}}K_{\mathrm{i}}}\left(\sin\vartheta\sin\varphi\frac{\partial n_{\mathrm{n}}}{\partial\tau} + \cos\vartheta\frac{\partial n_{\mathrm{n}}}{\partial\nu}\right)\Bigg), \tag{26}$$

where the subscript 0 is omitted. If the total macroscopic cross-section is large, the exponential term $e^{-\Sigma_{\mathrm{t}}(v)r_0}$ decays rapidly. Therefore, only the first mean free paths starting from the boundary contribute to the semi-infinite integral of Eq. (23). As long as the spatial variation of the parameters in the integrand is limited and the neutral density is approximately linear in this region, the assumptions are valid.

3.2. Distribution of the incident ions

The velocity- and angular dependent particle flux density of the incident ions is given by

$$\Gamma^{\mathrm{i}}_{\nu-}(v,\vartheta,\varphi) = \begin{cases} C^{\mathrm{i}}\widetilde{f}_{\mathrm{i}}(v,\vartheta,\varphi;\delta^{\mathrm{pot}}_{\mathrm{sh}})v\sin\vartheta\cos\vartheta & \text{if} \quad v \geq v_{\min}, \vartheta \leq \arccos\left(\frac{v_{\min}}{v}\right), \\ 0 & \text{else,} \end{cases} \tag{27}$$

with $v_{\min} = \sqrt{\frac{2}{m}\delta^{\mathrm{pot}}_{\mathrm{sh}}T_{\mathrm{e}}}$ the minimum occurring speed after the sheath acceleration. If the boundary is parallel to the magnetic field, $\delta^{\mathrm{pot}}_{\mathrm{sh}} = 0$. The coefficient C^{i} follows from following condition:

$$\int_{v=0}^{\infty}\int_{\vartheta=0}^{\pi/2}\int_{\varphi=0}^{2\pi}\Gamma^{\mathrm{i}}_{\nu-}(v,\vartheta,\varphi)\mathrm{d}v\mathrm{d}\vartheta\mathrm{d}\varphi = -n_{\mathrm{i}}u_{\nu}. \tag{28}$$

3.3. Boundary fluxes

From the distributions of the incident neutrals and ions, the net fluxes at the boundaries are calculated. In our case the recycling and reflection physics is determined by the TRIM code database. We elaborate the particle flux density in Section 3.3.1, the parallel momentum flux density in Section 3.3.2 and the energy flux density in Section 3.3.3. The resulting fluxes are imposed as boundary conditions for respectively the continuity (Eq. (5) and Eq. (15) for the pressure-diffusion equation (model 1)), the parallel momentum (Eq. (17)) and energy equation (Eq. (20)).

3.3.1. Particle flux density The net particle flux density $\Gamma^{\mathrm{n}} = \mathbf{\Gamma}^{\mathrm{n}}\cdot\boldsymbol{\nu}$, with $\boldsymbol{\nu}$ the inward pointing surface (unit) normal, becomes

$$\begin{aligned}\Gamma^{\mathrm{n}} = \int_{v=0}^{\infty}\int_{\vartheta=0}^{\pi/2}\int_{\varphi=0}^{2\pi}\big[&(-1+R^{\mathrm{n}}R(v,\vartheta)+R^{\mathrm{n}}R_{\mathrm{T}}(1-R(v,\vartheta)))\Gamma^{\mathrm{n}}_{\nu-}(v,\vartheta,\varphi) \\ &+(R^{\mathrm{i}}R(v,\vartheta)+R^{\mathrm{i}}R_{\mathrm{T}}(1-R(v,\vartheta)))\Gamma^{\mathrm{i}}_{\nu-}(v,\vartheta,\varphi)\big]\,\mathrm{d}v\mathrm{d}\vartheta\mathrm{d}\varphi,\end{aligned} \tag{29}$$

with $R(v,\vartheta)$ the reflection coefficient from the TRIM code database, which is a function of the energy (or speed) and angle with respect to the surface normal of the incident particle. The first line of the equation is the reflected minus the incident particle flux density, whereas the second line is the recycled particle flux density. A fraction R_{T} of the non-fast recycled/reflected neutrals, as described by the TRIM database, is emitted as dissociated 2 eV neutrals (due to Franck-Condon dissociation of the molecules). Finally, we have introduced the recycling and reflection coefficients (respectively R^{i} and R^{n}) to mimic the absorption of a fraction of the incident ions and neutrals, e.g., due to the presence of a pump. This particle flux density (and also the upcoming momentum and energy flux densities) are calculated in every boundary cell. In this way the coefficients R^{i}, R^{n} and R_{T} can depend on the position on a particular boundary. The coefficients from the TRIM code database are determined by the boundary material.

3.3.2. Parallel momentum flux density The parallel momentum flux density $\Gamma^{\mathrm{n}}_{\mathrm{m},||} = [\Gamma^{\mathrm{n}}_{\mathrm{m}} \cdot \boldsymbol{\nu}]_{||}$ becomes

$$\begin{aligned}\Gamma^{\mathrm{n}}_{\mathrm{m},||} =& m \int_{v=0}^{\infty} \int_{\vartheta=0}^{\pi/2} \int_{\varphi=0}^{2\pi} \Bigg[- v_{||} \Gamma^{\mathrm{n}}_{\nu-}(v,\vartheta,\varphi) + \int_{v_{\mathrm{R}}=0}^{v} \int_{\vartheta_{\mathrm{R}}=0}^{\pi/2} \int_{\varphi_{\mathrm{R}}=0}^{2\pi} v_{||,\mathrm{R}} \\ & R(v,\vartheta,\varphi \rightarrow v_{\mathrm{R}},\vartheta_{\mathrm{R}},\varphi_{\mathrm{R}}) \sin\vartheta_{\mathrm{R}} \mathrm{d}v_{\mathrm{R}} \mathrm{d}\vartheta_{\mathrm{R}} \mathrm{d}\varphi_{\mathrm{R}} \left(R^{\mathrm{n}} \Gamma^{\mathrm{n}}_{\nu-}(v,\vartheta,\varphi) \right. \\ & \left. + R^{\mathrm{i}} \Gamma^{\mathrm{i}}_{\nu-}(v,\vartheta,\varphi) \right) \Bigg] \mathrm{d}v \mathrm{d}\vartheta \mathrm{d}\varphi + \Gamma^{\mathrm{n}}_{\mathrm{m},||,\mathrm{T}}, \end{aligned} \tag{30}$$

with $v_{||} = b_\theta(\sin\alpha v_\tau + \cos\alpha v_\nu) + \sqrt{1-b_\theta^2} v_\phi$ the particle velocity parallel to the magnetic field, with α the angle between the surface normal and the poloidal direction and $\begin{bmatrix} v_\phi & v_\tau & v_\nu \end{bmatrix}^T$ the particle velocity expressed in the (ϕ,τ,ν) coordinate system. The probability that a particle with speed v, incident polar angle ϑ and azimuthal angle φ gets after the reflection a speed between v_{R} and $v_{\mathrm{R}} + \mathrm{d}v_{\mathrm{R}}$ and is scattered in the solid angle $\mathrm{d}\Omega_{\mathrm{R}} = \sin\vartheta_{\mathrm{R}} \mathrm{d}\vartheta_{\mathrm{R}} \mathrm{d}\varphi_{\mathrm{R}}$ is given by $R(v,\vartheta,\varphi \rightarrow v_{\mathrm{R}},\vartheta_{\mathrm{R}},\varphi_{\mathrm{R}}) \mathrm{d}v_{\mathrm{R}} \mathrm{d}\Omega_{\mathrm{R}}$. The first term in Eq. (30) represents the contribution of the incident neutrals, the second term of the fast recycled/reflected neutrals and $\Gamma^{\mathrm{n}}_{\mathrm{m},||,\mathrm{T}}$ the thermally released 2 eV neutrals. Eq. (30) can be simplified making use of the momentum reflection coefficients, defined as

$$\begin{aligned} R_{\mathrm{m},||}(v,\vartheta) =& \frac{1}{mv\sin\vartheta} \int_{v_{\mathrm{R}}=0}^{v} \int_{\vartheta_{\mathrm{R}}=0}^{\pi/2} \int_{\varphi_{\mathrm{R}}=0}^{2\pi} m v_{\mathrm{R}} \sin\vartheta_{\mathrm{R}} \cos\varphi_{\mathrm{R}} R(v,\vartheta,0 \rightarrow v_{\mathrm{R}},\vartheta_{\mathrm{R}},\pi+\varphi_{\mathrm{R}}) \\ & \sin\vartheta_{\mathrm{R}} \mathrm{d}v_{\mathrm{R}} \mathrm{d}\vartheta_{\mathrm{R}} \mathrm{d}\varphi_{\mathrm{R}}, \end{aligned} \tag{31}$$

$$\begin{aligned} R_{\mathrm{m},\perp}(v,\vartheta) =& \frac{1}{mv\cos\vartheta} \int_{v_{\mathrm{R}}=0}^{v} \int_{\vartheta_{\mathrm{R}}=0}^{\pi/2} \int_{\varphi_{\mathrm{R}}=0}^{2\pi} m v_{\mathrm{R}} \cos\vartheta_{\mathrm{R}} R(v,\vartheta,0 \rightarrow v_{\mathrm{R}},\vartheta_{\mathrm{R}},\pi+\varphi_{\mathrm{R}}) \\ & \sin\vartheta_{\mathrm{R}} \mathrm{d}v_{\mathrm{R}} \mathrm{d}\vartheta_{\mathrm{R}} \mathrm{d}\varphi_{\mathrm{R}}. \end{aligned} \tag{32}$$

The parallel momentum reflection coefficient $R_{\mathrm{m},||}(v,\vartheta)$ represents the mean fraction of momentum that is conserved in the direction of motion of the incident particle projected on the boundary plane multiplied by the probability of fast reflection $R(v,\vartheta)$. The perpendicular momentum reflection coefficient $R_{\mathrm{m},\perp}(v,\vartheta)$ represents the ratio of the momentum perpendicular to the plane of the reflected and incident particle again multiplied by $R(v,\vartheta)$. Both momentum reflection coefficients can be extracted from the TRIM code database as a function of the speed v and angle ϑ of the incident particle.

The thermally released neutrals are emitted isotropically (Lambert's cosine law), leading to the following parallel momentum flux density:

$$\begin{aligned} \Gamma^{\mathrm{n}}_{\mathrm{m},||,\mathrm{T}} =& b_\theta \cos\alpha \frac{2}{3} m v_{\mathrm{T}} R_{\mathrm{T}} \int_{v=0}^{\infty} \int_{\vartheta=0}^{\pi/2} \int_{\varphi=0}^{2\pi} (1 - R(v,\vartheta)) (R^{\mathrm{n}} \Gamma^{\mathrm{n}}_{\nu-}(v,\vartheta,\varphi) + R^{\mathrm{i}} \Gamma^{\mathrm{i}}_{\nu-}(v,\vartheta,\varphi)) \\ & \mathrm{d}v \mathrm{d}\vartheta \mathrm{d}\varphi, \end{aligned} \tag{33}$$

with v_{T} the speed of the thermally released atoms (corresponding to an energy of 2 eV).

The resulting parallel momentum flux density becomes

$$\begin{aligned}\Gamma^{\mathrm{n}}_{\mathrm{m},||} =& m\int_{v=0}^{\infty}\int_{\vartheta=0}^{\pi/2}\int_{\varphi=0}^{2\pi}\Bigg[-v_{||}\Gamma^{\mathrm{n}}_{\nu-}(v,\vartheta,\varphi)+\Bigg(-\sqrt{1-b_\theta^2}R_{\mathrm{m},||}(v,\vartheta)\sin\vartheta\cos\varphi\\ &-b_\theta\sin\alpha R_{\mathrm{m},||}(v,\vartheta)\sin\vartheta\sin\varphi+b_\theta\cos\alpha R_{\mathrm{m},\perp}(v,\vartheta)\cos\vartheta\Bigg)v\\ &\left(R^{\mathrm{n}}\Gamma^{\mathrm{n}}_{\nu-}(v,\vartheta,\varphi)+R^{\mathrm{i}}\Gamma^{\mathrm{i}}_{\nu-}(v,\vartheta,\varphi)\right)\Bigg]\mathrm{d}v\mathrm{d}\vartheta\mathrm{d}\varphi+\Gamma^{\mathrm{n}}_{\mathrm{m},||,\mathrm{T}}. \end{aligned} \tag{34}$$

As already mentioned in Section 2.2, there is an important distinction between the momentum flux density from the fluid approach (subscript f), which excludes the pressure, whereas the pressure is included in the momentum flux density from the kinetic point of view. Thus, the pressure is included in Eq. (34). However, as a boundary flux we impose $\Gamma^{\mathrm{n}}_{\mathrm{m,f},||}=\left[\Gamma^{\mathrm{n}}_{\mathrm{m,f}}\cdot\boldsymbol{\nu}\right]_{||}=\Gamma^{\mathrm{n}}_{\mathrm{m},||}-b_\theta\cos\alpha p_{\mathrm{n}}$.

There are two possible choices for the pressure at a certain position at a boundary. You can take the pressure that follows from the fluid solution. However, at the boundaries the underlying velocity distribution deviates a lot from the Maxwellian equilibrium distribution. Therefore, it is recommended to recalculate the pressure from the estimated distribution that consists of the incident, recycled and reflected neutrals. If the total velocity-dependent particle flux density at a boundary is $\Gamma^{\mathrm{n}}(\mathbf{v})$, the pressure is defined as

$$p_{\mathrm{n}}=\frac{m}{3}\int||\mathbf{v}-\mathbf{V}_{\mathrm{n}}||^2\frac{\Gamma^{\mathrm{n}}(\mathbf{v})}{|v_\nu|}\mathrm{d}\mathbf{v}. \tag{35}$$

Elaborating this for the estimated distribution, gives

$$\begin{aligned}p_{\mathrm{n}}\approx&\frac{m}{3}\int_{v=0}^{\infty}\int_{\vartheta=0}^{\pi/2}\int_{\varphi=0}^{2\pi}\Bigg[\left(v^2+2u_{\mathrm{n}\phi}v\sin\vartheta\cos\varphi+2u_{\mathrm{n}\tau}v\sin\vartheta\sin\varphi+2u_{\mathrm{n}\nu}v\cos\vartheta+u^2_{\mathrm{n}\phi}\right)\\ &\frac{\Gamma^{\mathrm{n}}_{\nu-}(v,\vartheta,\varphi)}{v\cos\vartheta}+\big(R_{p,1}(v,\vartheta)v^2+2u_{\mathrm{n}\phi}R_{p,2}(v,\vartheta)v\sin\vartheta\cos\varphi\\ &+2u_{\mathrm{n}\tau}R_{p,2}(v,\vartheta)v\sin\vartheta\sin\varphi-2u_{\mathrm{n}\nu}R(v,\vartheta)v\cos\vartheta+u^2_{\mathrm{n}\phi}R_{p,3}(v,\vartheta)\big)\\ &\frac{R^{\mathrm{n}}\Gamma^{\mathrm{n}}_{\nu-}(v,\vartheta,\varphi)+R^{\mathrm{i}}\Gamma^{\mathrm{i}}_{\nu-}(v,\vartheta,\varphi)}{v\cos\vartheta}\Bigg]\mathrm{d}v\mathrm{d}\vartheta\mathrm{d}\varphi+p_{\mathrm{n,T}}, \end{aligned} \tag{36}$$

with $\begin{bmatrix}u_{\mathrm{n}\phi} & u_{\mathrm{n}\tau} & u_{\mathrm{n}\nu}\end{bmatrix}^T$ the neutral fluid velocity expressed in the (ϕ,τ,ν) coordinate

system. Here, the pressure reflection coefficients are introduced. They are defined as

$$R_{p,1}(v,\vartheta) = \frac{\cos\vartheta}{v}\int_{v_\mathrm{R}=0}^{v}\int_{\vartheta_\mathrm{R}=0}^{\pi/2}\int_{\varphi_\mathrm{R}=0}^{2\pi}\frac{v_\mathrm{R}}{\cos\vartheta_\mathrm{R}}R(v,\vartheta,0\rightarrow v_\mathrm{R},\vartheta_\mathrm{R},\pi+\varphi_\mathrm{R})\sin\vartheta_\mathrm{R}\,\mathrm{d}v_\mathrm{R}\mathrm{d}\vartheta_\mathrm{R}\mathrm{d}\varphi_\mathrm{R}, \tag{37}$$

$$R_{p,2}(v,\vartheta) = \frac{1}{\tan\vartheta}\int_{v_\mathrm{R}=0}^{v}\int_{\vartheta_\mathrm{R}=0}^{\pi/2}\int_{\varphi_\mathrm{R}=0}^{2\pi}\tan\vartheta_\mathrm{R}\cos\varphi_\mathrm{R}R(v,\vartheta,0\rightarrow v_\mathrm{R},\vartheta_\mathrm{R},\pi+\varphi_\mathrm{R})\sin\vartheta_\mathrm{R}\,\mathrm{d}v_\mathrm{R}\mathrm{d}\vartheta_\mathrm{R}\mathrm{d}\varphi_\mathrm{R}, \tag{38}$$

$$R_{p,3}(v,\vartheta) = v\cos\vartheta\int_{v_\mathrm{R}=0}^{v}\int_{\vartheta_\mathrm{R}=0}^{\pi/2}\int_{\varphi_\mathrm{R}=0}^{2\pi}\frac{1}{v_\mathrm{R}\cos\vartheta_\mathrm{R}}R(v,\vartheta,0\rightarrow v_\mathrm{R},\vartheta_\mathrm{R},\pi+\varphi_\mathrm{R})\sin\vartheta_\mathrm{R}\,\mathrm{d}v_\mathrm{R}\mathrm{d}\vartheta_\mathrm{R}\mathrm{d}\varphi_\mathrm{R}. \tag{39}$$

Eq. (36) only approximates Eq. (35), because it is assumed that $u_{\mathrm{n}\phi} \gg u_{\mathrm{n}\tau}, u_{\mathrm{n}\nu}$, such that the square terms of $u_{\mathrm{n}\tau}$ and $u_{\mathrm{n}\nu}$ can be neglected. This assumption is equivalent to the parallel momentum equation (Eq. (17)), where it is assumed that the neutral parallel velocity is at least an order of magnitude larger than the radial and diamagnetic components. For small pitches the toroidal and parallel components are almost the same.

Finally, the pressure of the thermally released neutrals $p_{\mathrm{n,T}}$ becomes

$$p_{\mathrm{n,T}} \approx \frac{2}{3}m(v_\mathrm{T}-u_{\mathrm{n}\nu}+\frac{u_{\mathrm{n}\phi}^2}{v_\mathrm{T}})R_\mathrm{T}\int_{v=0}^{\infty}\int_{\vartheta=0}^{\pi/2}\int_{\varphi=0}^{2\pi}(1-R(v,\vartheta))(R^\mathrm{n}\Gamma^\mathrm{n}_{\nu-}(v,\vartheta,\varphi) + R^\mathrm{i}\Gamma^\mathrm{i}_{\nu-}(v,\vartheta,\varphi))\mathrm{d}v\mathrm{d}\vartheta\mathrm{d}\varphi. \tag{40}$$

3.3.3. Energy flux density The net energy flux density $Q^\mathrm{n} = \mathbf{Q}^\mathrm{n}\cdot\boldsymbol{\nu}$ becomes

$$\begin{aligned} Q^\mathrm{n} =& \frac{m}{2}\int_{v=0}^{\infty}\int_{\vartheta=0}^{\pi/2}\int_{\varphi=0}^{2\pi}\Bigg[-v^2\Gamma^\mathrm{n}_{\nu-}(v,\vartheta,\varphi)+\int_{v_\mathrm{R}=0}^{v}\int_{\vartheta_\mathrm{R}=0}^{\pi/2}\int_{\varphi_\mathrm{R}=0}^{2\pi}v_\mathrm{R}^2R(v,\vartheta,\varphi\rightarrow v_\mathrm{R},\vartheta_\mathrm{R},\varphi_\mathrm{R}) \\ & \sin\vartheta_\mathrm{R}\mathrm{d}v_\mathrm{R}\mathrm{d}\vartheta_\mathrm{R}\mathrm{d}\varphi_\mathrm{R}(R^\mathrm{n}\Gamma^\mathrm{n}_{\nu-}(v,\vartheta,\varphi)+R^\mathrm{i}\Gamma^\mathrm{i}_{\nu-}(v,\vartheta,\varphi))\Bigg]\mathrm{d}v\mathrm{d}\vartheta\mathrm{d}\varphi+Q^\mathrm{n}_\mathrm{T} \end{aligned} \tag{41}$$

$$\begin{aligned} =& \frac{m}{2}\int_{v=0}^{\infty}\int_{\vartheta=0}^{\pi/2}\int_{\varphi=0}^{2\pi}\Bigg[-v^2\Gamma^\mathrm{n}_{\nu-}(v,\vartheta,\varphi)+R_E(v,\vartheta)v^2(R^\mathrm{n}\Gamma^\mathrm{n}_{\nu-}(v,\vartheta,\varphi) \\ & + R^\mathrm{i}\Gamma^\mathrm{i}_{\nu-}(v,\vartheta,\varphi)\Bigg]\mathrm{d}v\mathrm{d}\vartheta\mathrm{d}\varphi+Q^\mathrm{n}_\mathrm{T}, \end{aligned} \tag{42}$$

making use of the energy reflection coefficient $R_E(v,\vartheta)$, defined as

$$R_E(v,\vartheta) = \frac{1}{mv^2/2}\int_{v_\mathrm{R}=0}^{v}\int_{\vartheta_\mathrm{R}=0}^{\pi/2}\int_{\varphi_\mathrm{R}=0}^{2\pi}\frac{m}{2}v_\mathrm{R}^2R(v,\vartheta,0\rightarrow v_\mathrm{R},\vartheta_\mathrm{R},\pi+\varphi_\mathrm{R})\sin\vartheta_\mathrm{R}\mathrm{d}v_\mathrm{R}\mathrm{d}\vartheta_\mathrm{R}\mathrm{d}\varphi_\mathrm{R}. \tag{43}$$

The energy flux density of the thermally released neutrals $Q_{\mathrm{T}}^{\mathrm{n}}$ becomes

$$Q_{\mathrm{T}}^{\mathrm{n}} = \frac{m}{2} v_{\mathrm{T}}^2 R_{\mathrm{T}} \int_{v=0}^{\infty} \int_{\vartheta=0}^{\pi/2} \int_{\varphi=0}^{2\pi} (1 - R(v,\vartheta))(R^{\mathrm{n}} \Gamma_{\nu-}^{\mathrm{n}}(v,\vartheta,\varphi) + R^{\mathrm{i}} \Gamma_{\nu-}^{\mathrm{i}}(v,\vartheta,\varphi)) \, \mathrm{d}v \mathrm{d}\vartheta \mathrm{d}\varphi. \tag{44}$$

3.4. Practical implementation

A three-dimensional integral over the whole velocity space has to be evaluated to calculate the different boundary fluxes. Due to the lack of analytic expressions, this has to be done numerically for each boundary cell and the calculation has to be repeated each time the plasma state changes. To avoid the computational cost to evaluate the integrals, they are calculated in advance for different values of the influencing plasma variables. Every boundary flux Γ_j^{n} can be written as

$$\Gamma_j^{\mathrm{n}} = \Gamma_{j,\nu-}^{\mathrm{n}} + \sum_k A_j^k \int_{v=0}^{\infty} \int_{\vartheta=0}^{\pi/2} \int_{\varphi=0}^{2\pi} g_j^k(v,\vartheta,\varphi;\mathbf{R}) \widetilde{f}_{\mathrm{i}}(v,\vartheta,\varphi;\delta_{\mathrm{sh}}^{\mathrm{pot},k},\mathbf{V}_{\mathrm{i}},T_{\mathrm{i}}) \mathrm{d}v \mathrm{d}\vartheta \mathrm{d}\varphi, \tag{45}$$

where the index j indicates the particular moment: 0 for the particle flux density Γ^{n}, 1 for the parallel momentum flux density $\Gamma_{\mathrm{m,f},||}^{\mathrm{n}}$ and 2 for the energy flux density Q^{n}. The coefficient A_i^j contains all terms that can be brought outside the integral (no function of v, ϑ or φ). The summation is used in order to distinguish between the different contributions. There is a contribution due to the recycled neutrals and three contributions of the reflected neutrals, respectively scaling with n_{n}, $\frac{\partial n_{\mathrm{n}}}{\partial \tau}$ and $\frac{\partial n_{\mathrm{n}}}{\partial \nu}$ (see Eq. (26)). Also the computation of the pressure leads to different contributions, e.g., terms scaling with $u_{\mathrm{n}\phi}$, $u_{\mathrm{n}\tau}$, $u_{\mathrm{n}\nu}$ and $u_{\mathrm{n}\phi}^2$ in Eq. (36). The integrand can be written as the product of a function $g_j^k(v,\vartheta,\varphi;\mathbf{R})$, which contains the needed TRIM reflection coefficients (present in $\mathbf{R}$), and the Maxwellian distribution $\widetilde{f}_{\mathrm{i}}(v,\vartheta,\varphi;\delta_{\mathrm{sh}}^{\mathrm{pot},k},\mathbf{V}_{\mathrm{i}},T_{\mathrm{i}})$ given by Eq. (22) (here we add explicitly the ion fluid velocity and temperature dependence of the Maxwellian distribution). The superscript k for $\delta_{\mathrm{sh}}^{\mathrm{pot}}$ is needed to distinguish between the recycled and reflected neutrals. For the reflected neutrals $\delta_{\mathrm{sh}}^{\mathrm{pot},k} = 0$, whereas $\delta_{\mathrm{sh}}^{\mathrm{pot},k}$ is nonzero for the recycled neutrals if the boundary is not fully parallel to the magnetic field. Only the integral in Eq. (45) is calculated in advance and saved as a function of the sheath transmission coefficient, ion fluid velocity and temperature:

$$I_j^k(\mathbf{V}_{\mathrm{i}},T_{\mathrm{i}}) = \int_{v=0}^{\infty} \int_{\vartheta=0}^{\pi/2} \int_{\varphi=0}^{2\pi} g_j^k(v,\vartheta,\varphi;\mathbf{R}) \widetilde{f}_{\mathrm{i}}(v,\vartheta,\varphi;\delta_{\mathrm{sh}}^{\mathrm{pot},k},\mathbf{V}_{\mathrm{i}},T_{\mathrm{i}}) \mathrm{d}v \mathrm{d}\vartheta \mathrm{d}\varphi. \tag{46}$$

To reduce the number of dependencies of I_j^k, we assume that $\mathbf{V}_{\mathrm{i}} \approx \begin{bmatrix} u_\phi & 0 & 0 \end{bmatrix}^T$, expressed in the (ϕ,τ,ν) coordinate system. This assumption is valid if the pitch is sufficiently small such that the parallel direction almost coincides with the toroidal direction and if the ion velocity perpendicular to the magnetic field lines is negligible, an assumption also made for the parallel momentum equation (Eq. (17)). In this way I_j^k contains all needed Maxwellian-averaged reflection coefficients for a discrete number of values for u_ϕ and T_{i}. We use linear interpolation for intermediate values of u_ϕ and T_{i}.

4. Comparison of the results from the fluid neutral models with the kinetic solution

In this section we compare the solutions of the different fluid neutral models (models 1 to 3) with the results from an MC simulation for the kinetic equation. The real ITER geometry is modeled and the fixed background plasma corresponds to a partially detached case. We use our in-house MC code, which is a simplified version of the full EIRENE code.

4.1. Description of the case

Fig. 2 shows a close-up of the ITER plasma edge near the X-point. The green shaded area corresponds to the simulation domain. We are only modeling the outer divertor leg. Besides the target boundary, the domain is bordered by the upstream, private flux (PF) and wall boundary. The private flux and wall boundaries do not correspond with the real vessel walls, but they coincide with some last simulated flux surfaces. In a traditional MC simulation the neutrals are tracked up to the real vessel wall. However, for our study we assume that the real vessel wall is located at the last simulated flux surfaces (both at the wall and private flux boundaries). Therefore, the sheath potential $\delta_{\mathrm{sh}}^{\mathrm{pot}} T_{\mathrm{e}}$ becomes zero at these boundaries. We assume that target, wall and private flux boundaries are made of carbon. All particles that reach the upstream boundary are absorbed, i.e., $R^{\mathrm{n}} = R^{\mathrm{i}} = 0$. For the other boundaries $R^{\mathrm{n}} = R^{\mathrm{i}} = 1$, except for the private flux boundary where $R^{\mathrm{n}} = 0.9$ due to the presence of a pump. The thermally released fraction R_{T} is 1 at all boundaries.

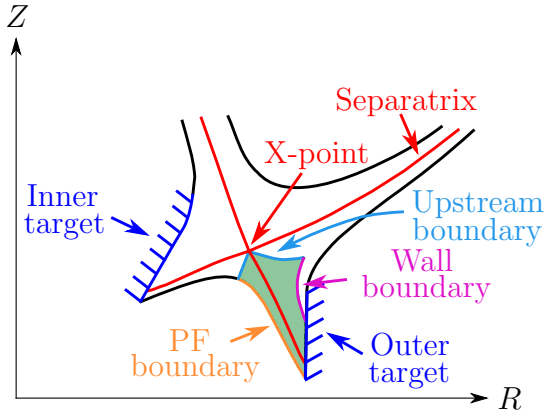

Figure 2. Location of the simulation domain (green shaded area).

Fig. 3 shows the fixed background plasma state and the magnetic pitch. The plasma state is a result from a simulation with B2-EIRENE for a partially detached case with an ITER F12 geometry [30]. The ion density peak is located a small distance from the target. The ion and electron densities and temperatures are assumed to be equal.

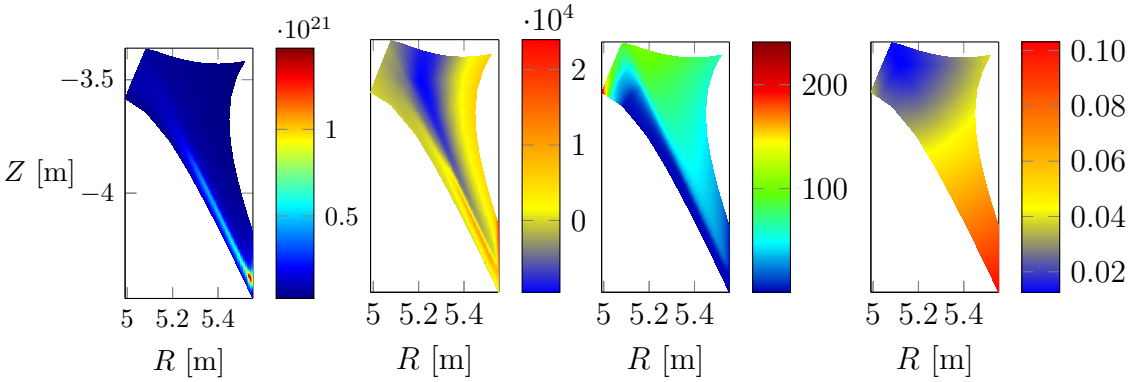

(a) Ion density [m^{-3}]. (b) Plasma parallel velocity [m/s]. (c) Ion temperature [eV]). (d) Magnetic pitch [-].

Figure 3. Plasma state and magnetic pitch. The ion and electron densities and temperatures are assumed to be equal.

4.2. Comparison of source terms

The most important outputs of the neutral model are the sources for the plasma. We compare the particle, parallel momentum and ion energy sources, respectively $S_{n_\mathrm{i}} = -S_{n_\mathrm{n}}$, $S_{mu_{||}} = -S_{mu_{\mathrm{n}||}}$ and $S_{E,\mathrm{i}} = -S_{E,\mathrm{n}}$.

Fig. 4 shows the sources from the MC simulation of the Boltzmann equation (Eq. (1)). The sources are dominant in a region close to the target. Only this region of the simulation domain is shown. The peak magnitude of the sources is located at the target plate. The global shapes of the sources from the fluid solutions are similar as the shapes from the MC solution. Therefore, to obtain a quantitative assessment we only compare the sources in single flux tubes. The selected flux tubes are indicated in Fig. 4. The peak particle source is located in the blue flux tube (1), the ion density peaks in the green flux tube (2) and the momentum source peaks in the red tube (3). The ion (and hence also the electron) density peak in the green flux tube leads to a local maximum of the ionization source.

The sources from the fluid models are compared to the kinetic solution in Fig. 5. They are plotted as a function of the poloidal distance from the target θ_t. All fluid models provide accurate predictions for the particle source with a maximum relative error of about 28% in the first cell adjacent to the target of the blue flux tube (tube 1). This flux tube is located in a high temperature region of the scrape-off layer that is much less CX dominated. This leads to larger errors close to the target due to the emission of non-equilibrium recycled/reflected neutrals.

From Figs. 5(b)-5(c) it is immediately clear that a parallel momentum equation has to be added to get qualitatively accurate results for the parallel momentum and ion energy sources. To not overload the figures, we only show the results for the red flux tube (3) where the peak momentum and energy sources are located, but the conclusions are also valid for the other flux tubes. The fluid models (with parallel momentum

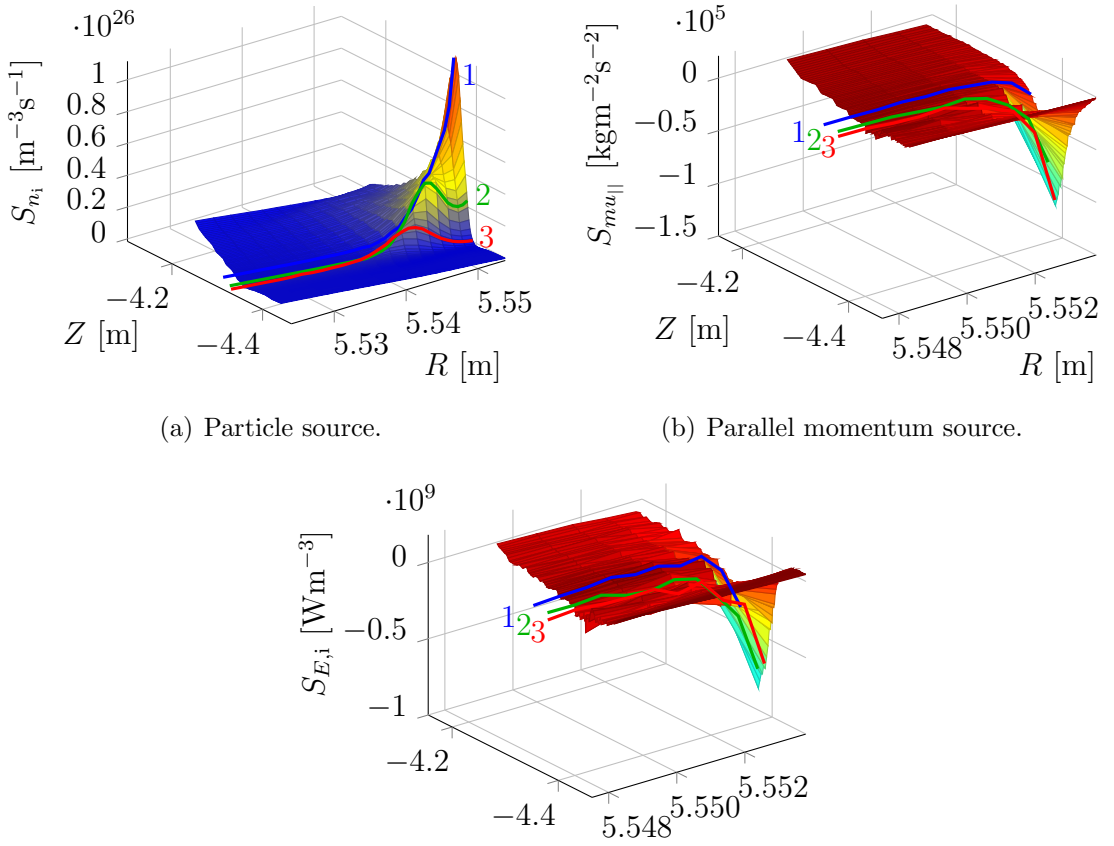

(a) Particle source.

(b) Parallel momentum source.

(c) Ion energy source.

Figure 4. Plasma sources from the MC simulation of the kinetic equation.

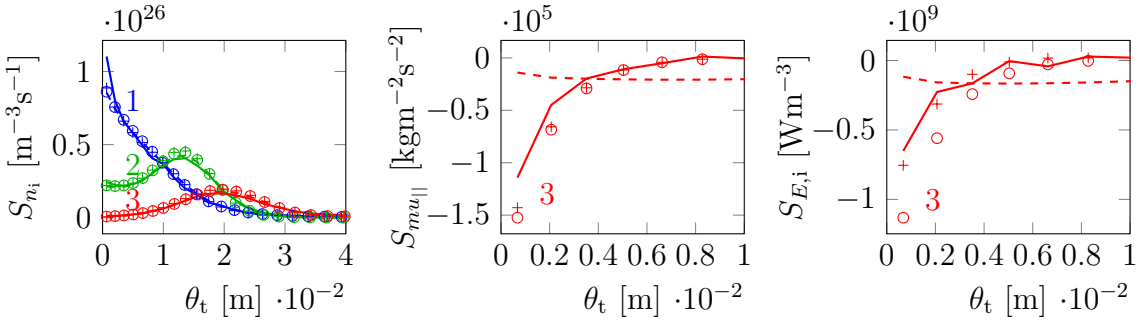

(a) Particle source.

(b) Parallel momentum source.

(c) Ion energy source.

Figure 5. Comparison of sources from fluid models with the MC solution: MC (solid line), pressure-diffusion equation (model 1) (dashed line), pressure-diffusion and parallel momentum equation (model 2) (circles) and pressure-diffusion, parallel momentum and energy equation (model 3) (pluses).

equation) overestimate the magnitude of the momentum and energy source close to the target. The relative errors of model 2 (no energy equation) for the momentum and energy source at the target plate in flux tube 3 are respectively 25 and 43%. These errors are reduced to respectively 20 and 14% by including a separate neutral energy

equation (model 3).

4.3. Comparison of state variables

We take a closer look to the individual state variables to clarify the differences between the results for the sources. For the particle source, the neutral density is the only influential parameter from the neutral solution, as can be seen in Eq. (10). Fig. 6(a) shows the neutral density profiles. The density differences between the fluid neutral models remain limited. Therefore, only the results from the MC simulation and fluid model 1 (pure pressure diffusion) are shown. The frequent CX collisions lead to an accumulation of neutrals in flux tubes 2 and 3. The fluid models underestimate the neutral density in the near vicinity of the target, also for flux tube 1 where it leads to an underestimate of the particle source. In tubes 2 and 3 the particle source peaks further away from the target. Therefore, the density inaccuracy close to the target has less impact on the particle source in these flux tubes. The density inaccuracies close to the target are caused by the emission of non-equilibrium recycled/reflected neutrals. It might sound surprising that the neutral density profiles from the different fluid models coincide what leads to almost equal particle sources. Due the toroidal symmetry, the particle transport is fully governed by the poloidal and radial fluxes. The poloidal transport is influenced by including a parallel momentum equation. However, due to the small magnetic pitch the influence of the parallel component on the poloidal flux is small compared to the diamagnetic contribution. The pressure-diffusion equation is used for the diamagnetic transport (Eq. (19)) for all models. Therefore, including a parallel momentum equation has only a minor influence on the particle transport, i.e., the neutral density solution.

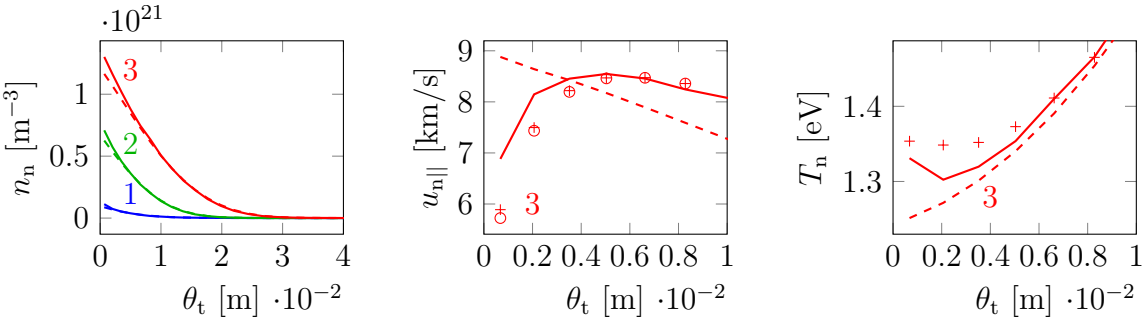

(a) Neutral density. (b) Neutral parallel velocity. (c) Neutral temperature.

Figure 6. Comparison of neutral state variables from fluid models with the MC solution: MC (solid line), pressure-diffusion equation (model 1) (dashed line), pressure-diffusion and parallel momentum equation (model 2) (circles) and pressure-diffusion, parallel momentum and energy equation (model 3) (pluses).

In contrast, the neutral parallel velocity is affected a lot by the parallel momentum equation as can be seen in Fig. 6(b). This significantly improves the results for the parallel momentum and ion energy source. Finally, Fig. 6(c) shows the neutral

temperature. Both models 1 and 2 assume the ion-neutral thermal equilibrium ($T_\mathrm{n} = T_\mathrm{i}$) (dashed line). The energy equation leads to a slight overestimate of the neutral temperature at the target plate, but the qualitative behavior is described correctly.

The accurate results close to the target are mainly due to the newly developed boundary conditions. All simulations from this paper are done with Carbon boundaries, but also for other materials with different TRIM reflection coefficients (e.g., Tungsten) the results for the fluid models are from the same order of accuracy.

4.4. Grid refinement

All previous simulations (Figs. 4-6) are done with a grid that consists of 120 cells in the poloidal and 200 cells in the radial direction. This is already about a factor 10 finer than one typically uses for plasma edge simulations of ITER. It should be noted that we exclusively simulate the outer divertor leg. Thus, the number of poloidal cells should be larger for a simulation of the whole plasma edge. These fine grids are inherent to the use of fluid neutral models that have to be able to capture the steep gradients of the neutral state variables near the target plate. This disadvantage of the fluid models is absent for the MC simulation, where the discretization error is typically smaller than the statistical error. However, when coupled to the plasma equations, the grid has to be sufficiently small to avoid large numerical errors for the plasma solution, but it is expected that the grid for the discretization of the plasma equations can be coarser in the vicinity of the target compared to the required grid for the fluid neutral models. It might be recommended to use different grids for the MC simulation and the fluid plasma or neutrals. A fine grid for the MC simulation would worsen the statistical properties.

Now, we double the number of cells in both poloidal and radial directions to estimate the discretization error. Fig. 7 shows the results for the parallel momentum and ion energy source for the red flux tube (3). The particle source is not influenced that much by the grid refinement and is omitted in Fig. 7. Because of the small discretization error of the MC solution, only the sources for the 120×200 grid are shown. The results from model 1 (pure pressure-diffusion equation) are not shown, because they are not accurate at all for the momentum and energy source. The results from the 240×400 grid are interpolated to the original 120×200 grid. The fluid solution approaches the kinetic solution for this grid refinement. The relative differences between the fluid and kinetic momentum source at the target are reduced to 9 and 6% for the 240×400 grid for respectively models 2 and 3 (originally they were 25 and 20%). There is only an improvement for the ion energy source for model 2, where the relative difference of the target source is reduced from 43 to 32%. The ion energy source from model 3 remains almost unchanged due to the fact that the results for both the neutral parallel velocity and temperature improve. The improved velocity leads to an increase of the energy source, whereas the temperature change leads to a decrease (Figs. 6(b)-6(c)). Both effects eliminate each other.

Though the fact that the 120×200 grid is already fine compared to typical plasma

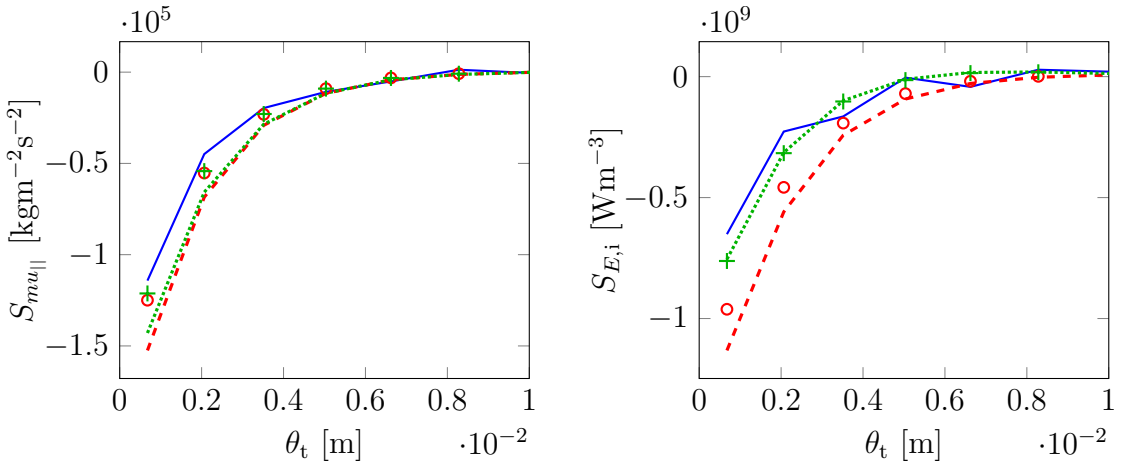

(a) Parallel momentum source.

(b) Ion energy source.

Figure 7. Comparison of sources for a grid refinement for flux tube 3: MC (solid line), model 2 with 120×200 grid (red dashed line), model 2 with 240×400 grid (red circles), model 3 with 120×200 grid (green dotted line) and model 3 with 240×400 grid (green pluses).

edge grids, it seems that there still remains a reasonable discretization error. The problem for a further refinement is the increase of the computational effort. Not only the time for a single iteration increases, but also the total number of iterations due to the increased stiffness of the discretized problem, i.e., the time step for the false time stepping procedure has to be lowered. The non-negligible discretization error is a disadvantage of the fluid neutral models, but we have proven that the fluid approximation becomes valid for this detached ITER case with a modeling error from the same order of magnitude as the discretization error. These accurate results are mainly obtained by the carefully elaborated boundary conditions.

5. Conclusions and future work

In this paper we have assessed different fluid neutral models by comparing the results with an MC simulation of the kinetic equation for a fixed background plasma that is typical for an ITER detached case. The pure pressure-diffusion equation predicts the particle source with a maximum error of 28% in the first cell near the target and about 10% further away from the target, but the model does not provide satisfying results for the parallel momentum and ion energy source, even not qualitatively. Therefore, we have added a parallel momentum equation. This leads to accurate results for the parallel momentum source (within 10% of accuracy) and ion energy source (maximum error of about 30%) in the flux tube where the peaks of momentum and energy source are located. The results further improve by adding a separate neutral energy equation (maximum error of about 6% for the momentum and 14% for the energy source).

We have shown that there still remains a reasonable discretization error for an

already relatively fine grid. The discretization error seems from the same order of magnitude as the modeling error. It is hard to exactly quantify the discretization and modeling errors due to the increased computational effort for a further refined mesh. However, we can conclude that the fluid models perform well for this detached case, mainly due to the newly developed boundary conditions, which translate the microscopic reflection model (TRIM in this case) in macroscopic boundary fluxes without the introduction of user-defined fitting parameters. We have derived fluid models that are fully consistent with the microscopic physics.

In future research, we plan to study the effect of molecules and neutral self-collisions. The convective term in the momentum equation might become important due to neutral-neutral collisions as discussed in Ref. [12] and the assumption of the dominant neutral velocity parallel to the magnetic field can be violated. Afterwards, the neutral model will be coupled to the plasma equations to study the effect on the plasma state. The presence of drifts can lead to significant diamagnetic ion and neutral velocities such that the parallel momentum equation has to be reformulated. We have assessed the fluid models for the Deuterium atoms. However, as future research it is worth the effort to study the performance of the fluid models for other species, e.g., Helium and Tungsten, and molecules.

If even more accurate results are desired, the fluid neutral model can be combined with a kinetic model. The efficiency of this combined fluid-kinetic hybrid model, i.e., the reduction of noise and calculation time, depends on the accuracy of the fluid part.

Acknowledgements

This work has been carried out within the framework of the EUROfusion Consortium and has received funding from the Euratom research and training programme 2014-2018 under grant agreement No 633053. The views and opinions expressed herein do not necessarily reflect those of the European Commission. The work of N. Horsten is supported by a PhD grant of the Research Foundation Flanders (FWO Vlaanderen).

References

[1] Reiter D, Baelmans M and Börner P 2005 *Fusion Science and Technology* **47** 172–186
[2] Dekeyser W 2013 *Optimal Plasma Edge Configurations for Next-Step Fusion Reactors* Ph.D. thesis KU Leuven
[3] Vold E L, Prinja A K, Najmabadi F and Conn R W 1992 *Fusion Science and Technology* **22** 208–226
[4] Hasan M Z and Conn R W 1987 *Journal of Computational Physics* **71** 371–390
[5] Umansky M, Rognlien T, Fenstermacher M, Borchardt M, Mutzke A, Riemann J, Schneider R and Owen L 2003 *Journal of nuclear materials* **313** 559–563
[6] Riemann J, Borchardt M, Schneider R, Mutzke A, Rognlien T and Umansky M 2004 *Contributions to Plasma Physics* **44** 35–38
[7] Hoshino K, Toma M, Hatayama A, Coster D, Bonnin X, Schneider R, Kawashima H, Asakura N and Suzuki Y 2008 *Contributions to Plasma Physics* **48** 136–140

[8] Furubayashi M, Hoshino K, Toma M, Hatayama A, Coster D, Schneider R, Bonnin X, Kawashima H, Asakura N and Suzuki Y 2009 *Journal of Nuclear Materials* **390** 295–298
[9] Wising F, Knoll D, Krasheninnikov S, Rognlien T and Sigmar D 1996 *Contributions to Plasma Physics* **36** 309–313
[10] Rensink M, Lodestro L, Porter G, Rognlien T and Coster D 1998 *Contributions to Plasma Physics* **38** 325–330
[11] Schneider R, Bonnin X, Borrass K, Coster D, Kastelewicz H, Reiter D, Rozhansky V and Braams B 2006 *Contributions to Plasma Physics* **46** 3–191
[12] Knoll D, McHugh P, Krasheninnikov S and Sigmar D 1996 *Physics of Plasmas* **3** 293–303
[13] Coster D, Bonnin X, Braams B, Reiter D, Schneider R *et al.* 2004 *Physica Scripta* **2004** 7
[14] Horsten N, Dekeyser W, Samaey G and Baelmans M 2016 *Physics of Plasmas (1994-present)* **23** 012510
[15] Reiter D 2000 The data file AMJUEL: Additional atomic and molecular data for EIRENE Tech. rep. FZ Juelich
[16] Reiter D 2002 The Data File HYDHEL: Atomic and Molecular Data for EIRENE Tech. rep. FZ Juelich
[17] Reiter D 2009 The EIRENE code user manual
[18] Karney C, Stotler D and Braams B 1998 *Contributions to Plasma Physics* **38** 319–324
[19] Horsten N, Dekeyser W, Samaey G and Baelmans M 2016 Submitted to Nuclear Materials and Energy
[20] Bobylev A 1982 The Chapman-Enskog and Grad methods for solving the Boltzmann equation *Akademiia Nauk SSSR Doklady* vol 262 pp 71–75
[21] Knoll D, Krasheninnikov S, McHugh P and Sigmar D 1996 *Physics of Plasmas (1994-present)* **3** 3358–3368
[22] Horsten N, Samaey G and Baelmans M 2016 *43rd European Physical Society Conference on Plasma Physics, Leuven*
[23] Rozhansky V, Voskoboynikov S, Kaveeva E, Coster D and Schneider R 2001 *Nuclear Fusion* **41** 387
[24] Wiesen S, Reiter D, Kotov V, Baelmans M, Dekeyser W, Kukushkin A, Lisgo S, Pitts R, Rozhansky V, Saibene G *et al.* 2015 *Journal of Nuclear Materials* **463** 480–484
[25] Baelmans M 1994 *Code improvements and applications of a two-dimensional edge plasma model for toroidal devices* Ph.D. thesis
[26] Horsten N, Dekeyser W, Samaey G, Boïner P and Baelmans M 2016 *Contributions to Plasma Physics* **56** 610–615 ISSN 1521-3986
[27] Espinosa-Paredes G, Polo-Labarrios M A, Espinosa-Martínez E G and Valle-Gallegos E d 2011 *Annals of Nuclear Energy* **38** 307–330
[28] Park H J, Shim H J, Joo H G and Kim C H 2012 *Nuclear science and engineering* **172** 66–77
[29] Piovezan P, Carluccio T, Abe A and Santos A d 2013
[30] Kukushkin A, Pacher H, Kotov V, Reiter D, Coster D and Pacher G 2007 *Nuclear fusion* **47** 698